2.2. *Experiment*

Measurements were carried out using the therapeutic proton beam line at National Cancer Center Hospital East in Japan. We adopt the dual-ring double-scattering methods (Nishio *et al* 2006). The thickness of the first scatter and the shape of the second scatter are determined by the energy of the proton beams. The maximum size of the irradiation field provided by this system is 200 mm ø. Proton beams with 190 MeV were used in this study.

We used the TN502RD MOSFET and a high sensitivity bias voltage supply. Measurements were carried out in an acrylic phantom for dose calibration and a cylindrical acrylic phantom for angular dependence measurement. A calibrated 0.6 cm^3 Farmer ionization chamber (IC) was placed along with the MOSFET in the dose calibration phantom. Except for fading-effect measurements, MOSFETs were read 10 s after each irradiation in order to perform a stable read-out without fading effect. Dose calibration was performed using a proton beam of LET = 0.5 keV μm^{-1}. Protons with LET = 0.5 keV μm^{-1} means protons in the proximal region of the Bragg curve.

Reproducibility, linearity measurement and proton radiation damage for the MOSFET response were measured. For reproducibility measurements, the MOSFET was exposed to 100 cGy ten times. The response was averaged and the standard deviation was calculated. In addition to ionizing proton losses (IEL), which lead to charge build up in the gate oxide, the MOSFET can suffer from non-ionizing energy losses (NIEL), producing displacement damage in the oxide and the bulk of silicon. Therefore, doses ranging from 100 cGy to 8000 cGy were applied to measure linearity and to observe proton radiation damage.

We also investigated the MOSFET response following irradiation as a function of the time difference between the time of irradiation and the read-out, to evaluate the fading effect. The MOSFET dosimeter was irradiated by a proton beam and the response was measured 3–900 seconds after irradiation. This procedure was repeated five times for each duration.

An effect of proton beam intensity on the MOSFET response was also measured. The beam intensity was varied from 0.5 nA to 13 nA. The LET of the radiated proton beam was 0.5 keV μm^{-1}. In addition, protons with LET = 1.8 KeV μm^{-1} near the Bragg peak were also irradiated. This procedure was also repeated five times for each proton beam intensity and each LET.

Previous studies investigated the angular dependence of the MOSFET (Chuang *et al* 2002, Rowbotton and Jaffray 2004, Ramaseshan *et al* 2004). They reported that the angular dependence for photon beams was within 2–3%. Wang *et al* (2004, 2005) simulated the angular dependence of the MOSFET response by the Monte Carlo method, and the angular dependence as a function of photon energy was evaluated. On the other hand, the angular dependence of the TN502RD MOSFET response for proton beams has never before been reported. Therefore, the dependence for proton beams was experimentally evaluated. As shown in figure 1, a cylindrical acrylic phantom with a radius of 8.0 cm was used for this measurement. The MOSFET dosimeter can rotate 360 degrees in the phantom. The angular MOSFET responses along the cable axis were measured every 45 degrees from 0 to 360 degrees.

Lastly, some literature has reported the energy dependence for photon beams. Ramaseshan *et al* (2004) reported that the response was uniform in the therapy region between 4 MV and 18 MV within the uncertainty. On the other hand, Edwards *et al* (1997) and Kron *et al* (1998) measured the energy dependence for low-energy photons, and found the MOSFET dosimeters overestimate dose at low energies. Additionally, Rosenfeld *et al* (2000) reported that the response of their MOSFET is dependent on the particle LET with respect to the oxide electric field. Thus, we expected the TN502RD MOSFET dosimeter to have LET dependence,

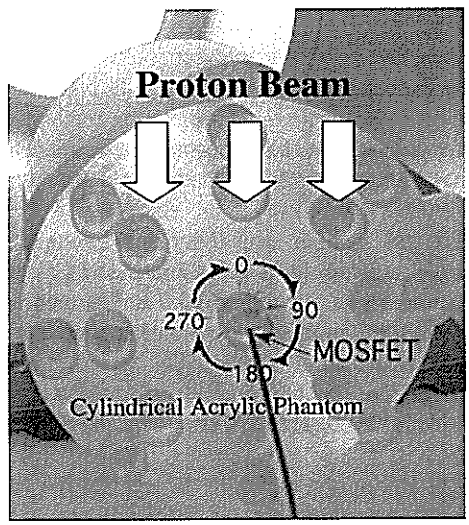

Figure 1. A cylindrical acrylic phantom with a radius of 10.0 cm was used for measurement of the angular dependence of the MOSFET response.

and were interested in the MOSFET response around the Bragg peak. The LET of a proton beam with 190 MeV changes continuously from 0.5 keV μm^{-1} to over 50 keV μm^{-1}. The depth–dose curve for a mono-energetic proton beam was measured by the MOSFET and the IC. The polyethylene slabs ranging from 0 mm to 175 mm were stacked on the acrylic phantom with the MOSFET and the IC. Measurements were repeated three times for each thickness.

Furthermore, the spread-out Bragg peak (SOBP) was also measured for a modulated proton beam. The SOBP can be obtained with a ridge-filter in a stepwise manner which changes beam weights and beam energies. The resulting Bragg peaks are stacked throughout the depth of the target.

3. Results

The linearity plot in figure 2 showed that the dose is linear up to 8000 cGy. Figure 2 shows that the MOSFET indicates good linearity of response. The reproducibility was found to be $\pm 1.5\%$ at one standard deviation. No proton damage effect was observed by changing the irradiation dose up to 8000 cGy. Temperature variation during these experiments was within ± 0.3 °C. As Cheung *et al* (2004) reported that the MOSFET provides stable dose measurements with temperature varying from 15 °C up to 40 °C, temperature effect on the MOSFET response did not affect trends in our measurements.

The fading effect is shown in figure 3. It is known that the radiation stored in a MOSFET fades as time goes by. Those data were normalized by the output after 3 s. When the MOSFETs were read 15 minutes after irradiation, we observed a fading effect of about 2.3%. Therefore, in this study, MOSFETs were read 10 s after each irradiation to give steady read-out without fading effect.

Proton beam intensity dependence of the MOSFET response is plotted in figure 4. No measurable effect was observed by changing the proton beam intensity for both LETs.

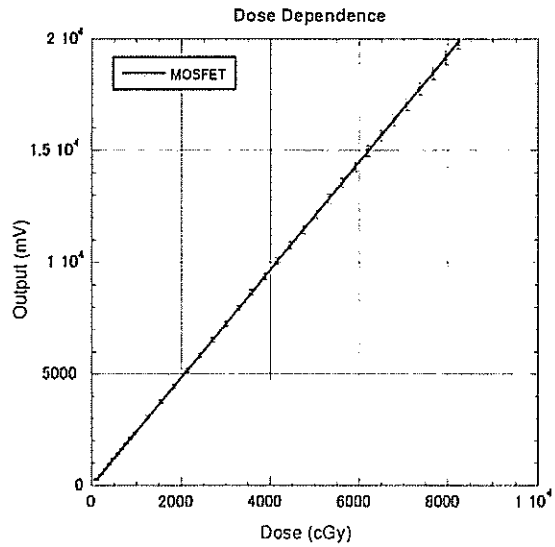

Figure 2. MOSFET linearity response for proton doses ranging from 0 cGy to 8000 cGy.

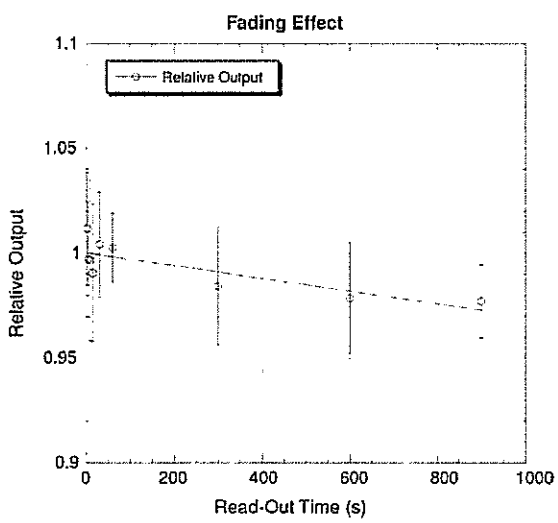

Figure 3. Fading effect of MOSFET response.

However, as shown in figure 4, the MOSFET response for LET = 1.8 keV μm^{-1} was 0.8 times as large as the MOSFET response for LET = 0.5 keV μm^{-1}. This made us expect the MOSFET response to have LET dependence.

Figure 5 shows angular dependence of the MOSFET response for a proton beam. The MOSFET responses were measured at every 45 degrees from 0 to 360 degrees. These were normalized to the response at 0 degrees. The angular MOSFET response of 180 degrees agreed well with those of 0 and 360 degrees within ±1.0%. On the other hand, the MOSFET

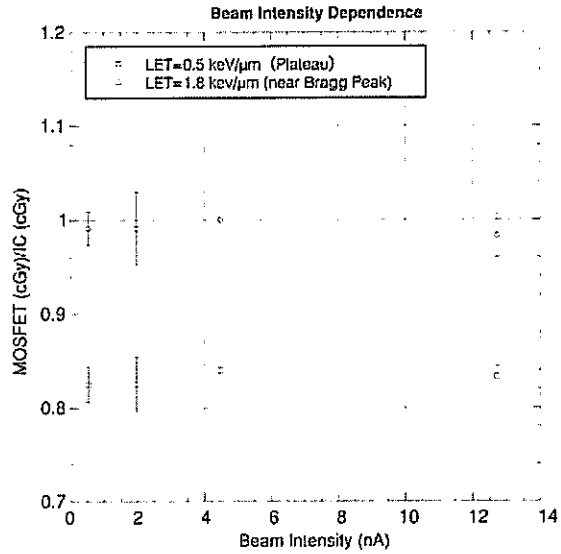

Figure 4. Proton beam intensity dependence of MOSFET response

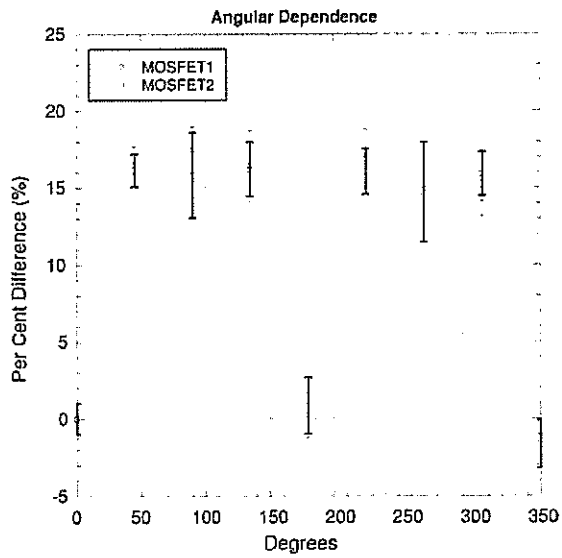

Figure 5. Angular dependence of MOSFET measured for a proton beam.

responses at 45, 90, 135, 225, 270 and 315 degrees for proton beams were over-responses of about +15%. Though some authors reported that angular dependence for photon beams is within 2.0%, these results for the proton beam were largely different from those of photon beams.

The comparison of the depth–dose distributions measured by the MOSFET dosimeter and the IC for the mono-energy proton beam is shown in figure 6. As expected from figure 4, there

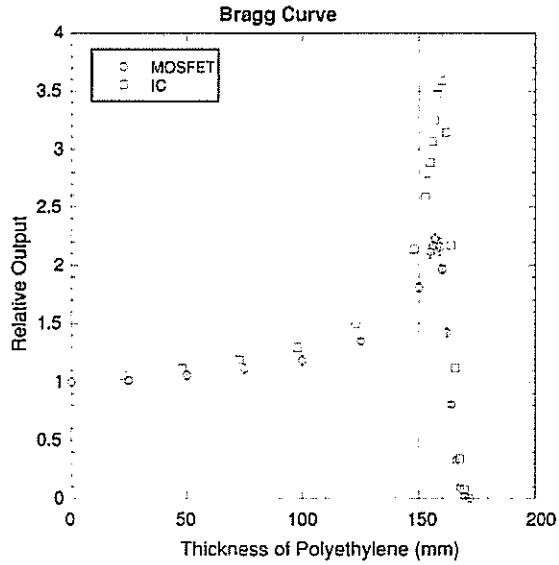

Figure 6. The comparison of the Bragg curve by the MOSFET dosimeter and the ionization chamber (IC) for a mono-energy proton beam.

is a notable disagreement between the two curves around the peak position of the Bragg curve. The MOSFET response decreases as it approaches the distal edge. The Bragg peaks obtained by the MOSFET were estimated to be about 40% lower than those by the ionization chamber. It was obvious that the MOSFET response depends strongly on the LET of protons. Figure 7 shows the comparison of the spread-out Bragg curve measured by the MOSFET dosimeter and the IC for a modulated proton beam. As expected, the SOBPs obtained by the MOSFET were also estimated to be more than 20% lower than those of the IC.

4. Discussion

Using the same phantom, we have already measured the angular dependence of the MOSFET response for photon beams, and found it to be within 2.9%. This result was the same as those for photon beams found by previous papers. We found that the angular dependence of the MOSFET for proton beams has no uncertainty of configuration of the cylindrical acrylic phantom. Namely, we guess that this angular dependence for proton beams is peculiar to protons.

For the result of the SOBP obtained by the MOSFET in figure 7, we simulated the SOBP formed by protons passed through a ridge-filter in a stepwise manner. In order to simulate the SOBP obtained by the MOSFET, we used the above-measured Bragg curve of the MOSFET in figure 6 for a mono-energetic proton beam. In figure 7, MOSFET:Simulation means the simulation of the SOBP. The SOBP measured by the MOSFET agreed well with the MOSFET:Simulation. This concludes that the measurement by the MOSFET is a proper result. We reconfirmed that the MOSFET response has an LET dependence for the SOBP beam as well as figure 6. Thus, it is obvious that the MOSFET response depends strongly on LET and angular dependence for proton beams.

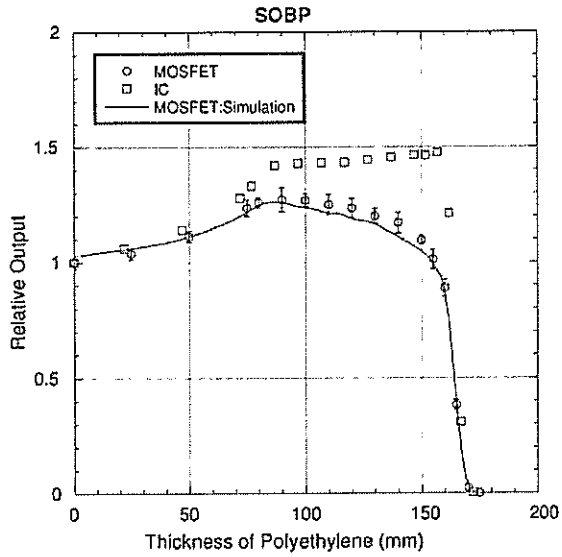

Figure 7. The comparison of the spread-out Bragg curve by the MOSFET dosimeter and the ionization chamber (IC) for a modulated proton beam. MOSFET:Simulation means SOBP simulated using the Bragg curve in figure 6 measured by the MOSFET.

These responses can be explained by the columnar recombination model (Tallon *et al* 1987). In a proton therapy with LET, the plasma track of electron–hole pairs generated by protons in the gate of the MOSFET becomes more dense, and recombination of electron–hole pairs in a track increases, leading to poor hole collection and reducing the MOSFET response with increasing LET.

Additionally, response of the MOSFET depends on the electrical field in the gate of the MOSFET and the direction of this field in relation to the proton beam. In the case of the MOSFET being irradiated with an epoxy cover facing the beam, the electrical field in the gate of the oxide is parallel to the plasma track produced by protons, and drift of electron–hole pairs due to the electrical field is not essential compared to diffusion of electron–hole pairs in a dense plasma track. This leads to an increased time of charge collection and strong recombination of electron–hole pairs in a track.

In case of 'edge on' MOSFET dosimetry (Rosenfeld *et al* 2001), the vector of the electrical field is perpendicular to the plasma track and the effect of the electrical field is essential, leading to faster drift of electron–hole pairs and reduction of recombination. This explains the angular dependence of the response of the MOSFET detector to the proton beam. In figure 5, the sensitivity of the MOSFET for 0, 180 and 360 degrees is less; that corresponds to the direction of the beam relative to the epoxy side or the kapton side of the MOSFET.

Ideally, these results of angular and LET dependence for proton beams may be confirmed by a Monte Carlo simulation. Furthermore, in order to improve these responses, we want to test smaller MOSFETs such as the microMOSFET for proton dosimetry. However, they are the subjects of future work.

5. Conclusion

We experimentally evaluated dose reproducibility, linearity, fading effect, beam intensity dependence, angular dependence and LET dependence for therapeutic proton beams. Many characteristics of the MOSFET response for protons were the same as those for photon beams reported by many authors. However, it was obvious that the MOSFET response had a large angular dependence of 17% for proton beams. Moreover, we found that the Bragg curve and SOBP measured by the MOSFET dosimeter were estimated to be 20–40% lower than those measured by the IC. In conclusion, it may be hard for quantitative proton dose measurements to use the MOSFET dosimeter due to angular dependence and LET dependence. We do not recommend the MOSFETs of this type for *in vivo* patient proton dosimetry.

Acknowledgments

We wish to thank Yu Igarashi, AcroBio Corporation, for his help with this work. We are grateful to Dr Abdelbasset Hallil, Best Medical Canada, for his useful discussion and technical support. The authors would also like to thank Kazutomo Matsumura, Hideki Saitoh, Toshinobu Sasano Naoya Uzawa and Toshio Nakamura, SHI Accelerator Service Ltd., for experimental support.

References

Cheung T, Butson M J and Yu P K N 2004 Effects of temperature variation on MOSFET dosimetry *Phys. Med. Biol.* 49 N191–6

Chuang C F, Verhey L J and Xia P 2002 Investigation of the use of MOSFET for clinical IMRT dosimetric verification *Med. Phys.* 29 1109–15

Edwards C R, Green S, Palethorpe J E and Mountford P J 1997 The response of a MOSFET, p-type semiconductor and LiF TLD to quasi-monoenergetic x-rays *Phys. Med. Biol.* 42 2383–91

Kohno R, Takada Y, Sakae T, Terunuma T, Matsumoto K, Nohtomi A and Matsuda H 2003 Experimental evaluation for validity of simplified Monte Carlo method in proton dose calculations *Phys. Med. Biol.* 48 1277–88

Kron T, Duggan L, Smith T, Rosenfeld A, Butson M, Kaplan G, Howlett S and Hyodo K 1998 Dose response of various radiation detectors to synchrotron radiation *Phys. Med. Biol.* 43 3235–59

Miller D W 1995 A review of proton beam radiation therapy *Med. Phys.* 22 1943–54

Nishio T, Kataoka S, Tachibana M, Matsumura K, Uzawa N, Saito H, Sasano T, Yamaguchi M and Ogino T 2006 Development of a simple control system for uniform proton dose distribution in a dual-ring double scattering method *Phys. Med. Biol.* **51** 1249–60

Ramaseshan R, Russell S and O'Brien P 1997 Clinical dosimetry using mosfets *Int. J. Radiat. Oncol. Biol. Phys.* 37 959–64

Ramaseshan R, Kohil K S, Zhang T J, Lam T, Norlinger B, Hallil A and Islam M 2004 Performance characteristics of a micro MOSFET as an in vivo dosimeter in radiation therapy *Phys. Med. Biol.* 49 4031–48

Rosenfeld A B, Bradley P D, Cornelius I, Kaplan G I, Allen B J, Flanz J B, Goitein M, Meerbeeck A V, Schbert J, Bailey J, Takada Y, Maruhashi A and Hayakawa Y 2000 New silicon detector for microdosimetry applications in proton therapy *IEEE Trans. Nucl. Sci.* 47 1386–94

Rosenfeld A B, Lerch M L F, Kron T, Brauer-Krisch E, Bravin A, Holmes-Siedle A and Allen B J 2001 Feasibility study of online high-spatial-resolution MOSFET dosimetry in static and pulsed x-ray radiation fields *IEEE Trans. Nucl. Sci.* 48 2061–8

Rosenfeld A B 2002 MOSFET dosimetry in modern radiation oncology modalities *Radiat. Prot. Dosim.* **101** 393–8

Rowbotton C G and Jaffray D A 2004 Characteristics and performance of a micro-MOSFET: an imageable dosimeter for image-guided radiotherapy *Med. Phys.* **31** 609–15

Soubra M, Cygler J and Mackay G 1994 Evaluation of a dual metal oxide semiconductor field-effect transistor detector as radiation dosimeter *Med. Phys.* 21 567–72

Tallon R W, Kemp W T, Ackermann M R, Owen M H and Hoffland A H 1987 Radiation damage in MOS transistors as a function of the angle between an applied electric field and various incident radiations (protons, electrons, and Co-60 gamma rays) *IEEE Trans. Nucl. Sci.* **34** 1208–13

Wang B, Kim C H and Xu X G 2004 Monte Carlo modeling of high-sensitivity MOSFET dosimeter for low- and medium-energy photon sources *Med. Phys.* **31** 1003–8

Wang B, Xu X G and Kim CH 2005 Montecarlo study of MOSFET dosemeter sharacteristics: dose dependence on photon energy, direction and dosemeter composition *Radiat. Prot. Dosim.* **113** 40–6

Int. J. Radiation Oncology Biol. Phys., Vol. 65, No. 1, pp. 107–111, 2006

0360-3016/06/$–see front matter

ELSEVIER

doi:10.1016/j.ijrobp.2005.10.031

CLINICAL INVESTIGATION **Lung**

HIGH-DOSE PROTON BEAM THERAPY FOR STAGE I NON–SMALL-CELL LUNG CANCER

KEIJI NIHEI, M.D., TAKASHI OGINO, M.D., SATOSHI ISHIKURA, M.D., AND HIDEKI NISHIMURA, M.D.

Radiation Oncology Division, National Cancer Center Hospital East, Kashiwa, Chiba, Japan

Purpose: To evaluate retrospectively the safety and efficacy of high-dose proton beam therapy (PBT) for Stage I non–small-cell lung cancer (NSCLC).

Methods and Materials: Between 1999 and 2003, 37 patients were treated in our institution. The indications for PBT were pathologically proven NSCLC, clinical Stage I, tumor size ≤5 cm, medically inoperable or refusal of surgery, and written informed consent. A total dose of 70–94 Gy_E was delivered in 20 fractions (3.5–4.9 Gy_E per fraction).

Results: Patient characteristics (number of patients) were as follows: Stage IA/IB, 17 of 20; medically inoperable/refusal of surgery, 23/14; total dose 70/80/88/94 Gy_E, 3/17/16/1. With a median follow-up period of 24 months, the 2-year local progression-free and overall survival rates were 80% and 84%, respectively. The 2-year locoregional relapse-free survival rates in Stage IA and Stage IB were 79% and 60%, respectively. No serious acute toxicity was observed. Late Grades 2 and 3 pulmonary toxicities were observed in 3 patients each. Of these 6 patients, 5 had Stage IB disease.

Conclusions: Proton beam therapy is a promising treatment modality for Stage I NSCLC, though locoregional relapse and late pulmonary toxicities in Stage IB patients were substantial. Further investigation of PBT for Stage I NSCLC is warranted. © 2006 Elsevier Inc.

Proton beam therapy, Radiotherapy, High dose, Non–small-cell lung cancer, Stage I.

INTRODUCTION

Lung cancer continues to be the leading cause of cancer death worldwide. Surgical resection for Stage I (T1–2N0) non–small-cell lung cancer (NSCLC) results in 5-year overall survival rates of approximately 60–70% and remains the standard treatment for this population (1, 2).

Some patients with Stage I NSCLC cannot undergo surgery, owing to preexisting comorbidities, advanced age, or refusal. Conventional radiotherapy alone has been used as the next alternative approach for these patients with early-stage NSCLC, but outcomes have been inferior to those of surgical resection (3–6), although there is a potential selection bias due to stage migration and patients' general conditions. Some studies reported a benefit of dose escalation, suggesting that higher doses of radiation therapy might improve both local tumor control and survival (7). However, conventional radiotherapy often cannot deliver higher doses to the tumor without increasing adverse effects.

Proton beams have a distinct physical advantage over conventional photon beams. Proton beams have a low entrance dose, a maximal dose at any prescribed depth, called the "Bragg peak," and no exit dose. The "Bragg peak" can be spread out and shaped to conform to the depth and volume of an irregular target. Proton beam therapy (PBT) can thus create an inherently three-dimensional conformal dose distribution without extra dose to the surrounding normal tissue compared with conformal photon treatment.

At the National Cancer Center Hospital East, we introduced PBT for clinical use in 1998. In the present study, we retrospectively evaluated the safety and efficacy of high-dose PBT for Stage I NSCLC.

METHODS AND MATERIALS

We started a Phase I dose escalation study of PBT for Stage I NSCLC in December 1999 for the purpose of determining the maximum tolerated dose. The eligibility criteria were (*1*) pathologically proven NSCLC, (*2*) clinical Stage I, (*3*) tumor size ≤5 cm in diameter, (*4*) pO_2 ≥60 torr, (*5*) medically inoperable or refusal of surgery, (*6*) Zubrod performance status 0–2, and (*7*) written informed consent. Patients received escalating doses of PBT in 20 fractions (fx) over 4 or 5 weeks as follows: level 1: 70 Gy_E (3.5 Gy_E/fx); level 2: 80 Gy_E (4.0 Gy_E/fx); level 3: 88 Gy_E (4.4 Gy_E/fx); level 4: 94 Gy_E (4.7 Gy_E/fx); level 5: 98 Gy_E (4.9 Gy_E/fx). Dose-limiting toxicity included Grade 4 radiation dermatitis and other Grade 3 nonhematologic toxicities.

Reprint requests to: Keiji Nihei, M.D., National Cancer Center Hospital East, Radiation Oncology Division, 6-5-1, Kashiwanoha, Kashiwa, Chiba, Japan. Tel: (+81) 4-7133-1111; Fax: (+81) 4-7131-4724; E-mail: knihei@east.ncc.go.jp

Presented at the 41st Annual Meeting of the American Society of Clinical Oncology, Orlando, Florida, May 13–17, 2005.

Received Aug 12, 2005, and in revised form Oct 7, 2005. Accepted for publication Oct 18, 2005.

In total, 10 patients were enrolled in the dose escalation study. Three patients were enrolled in each of levels 1 to 3. The first patient enrolled in level 4 (94 Gy_E) suffered symptomatic radiation pneumonitis after PBT, which resulted in early closure of the study. In July 2001, PBT in Japan was authorized by the government as a highly advanced medical technology, and thereafter an additional 27 patients who had met the criteria above were treated by PBT on an off-study basis. Thirteen of them received a total dose of 88 Gy_E (4.4 Gy_E/fx), and the other 14 patients with poorer pulmonary function received a total dose of 80 Gy_E (4.0 Gy_E/fx) at the discretion of the radiation oncologists.

For PBT planning, thoracic CT images were obtained in the exhalation phase with a respiratory gating system. Patients were immobilized in the supine position on a body cast with both arms above the head. The primary tumor was delineated on a lung window as the gross tumor volume. The clinical target volume was defined as the gross tumor volume with a margin of 8 mm in all directions for subclinical tumor extension. The planning target volume was defined as the clinical target volume with a setup margin of 5 mm and with an internal margin of 5 mm for uncertainty of respiratory motion. Two or four portals of proton beams were arranged in the optimal angles to avoid excessive dose exposure to the normal lung and skin. Range modulation by bar-ridge filters was used to generate Spread-Out Bragg Peak, and 150-MeV or 190-MeV proton beams were selected to conform to the target volume. Daily verification of patient positioning was performed by the image subtraction method with digital radiography (8). Respiratory gating was used in all patients during the treatment to deliver proton beams to the target volume in the exhalation phase. The relative biologic effectiveness of our proton beam was 1.1 (Gy_E = proton Gy × 1.1), according to a previous animal examination (9).

After PBT, patients were examined every 3 months for the first 2 years and every 6 months thereafter. Chest X-ray films and CT images were also obtained at the same time to evaluate the local tumor response and other radiographic findings.

Tumor response was evaluated according to the previously published Response Evaluation Criteria in Solid Tumors (10). A complete response indicated that the tumor had completely disappeared, and partial response was defined as ≥30% reduction in the maximum cross-sectional diameter. Although it was difficult to distinguish the residual tumor tissue from radiation fibrosis, the observed residual density was considered free of local progression unless its size subsequently increased.

The Kaplan-Meier method was used to assess survival. Acute toxicities were assessed by the Common Toxicity Criteria (version 2.0), and late toxicities were scored according to the European Organization for Research and Treatment of Cancer/Radiation Therapy Oncology Group late radiation morbidity scoring scheme.

Table 1. Patient characteristics

Median age (range) (y)	75 (63–87)
Men/women (*n*)	30/7
Clinical stage* (IA/IB) (*n*)	17/20
Histology (SCC/adeno/others) (*n*)	15/15/7
Medically inoperable/refusal of surgery (*n*)	23/14
Total dose (70/80/88/94 Gy_E) (*n*)	3/17/16/1

Abbreviations: SCC = squamous cell carcinoma; adeno = adenocarcinoma.

* TNM classification.

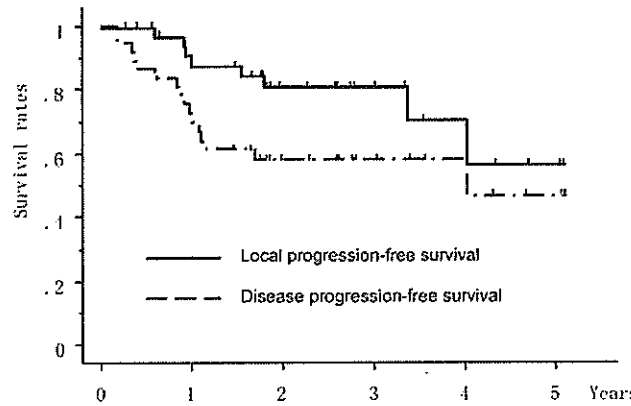

Fig. 1. Local progression-free and disease progression-free survival rates in all patients.

RESULTS

Between December 1999 and October 2003, 37 patients with Stage I NSCLC, including 10 patients enrolled in the dose escalation study, were treated by PBT in our institution. Patient characteristics are shown in Table 1.

The median duration of follow-up in all patients was 24 months (range, 3–62 months). The overall response rate was 86% (95% confidence interval [CI], 71–96%), but primary tumor regrowth occurred in 2 patients, at 7 and 12 months after treatment, respectively. The 1- and 2-year local progression-free survival rates, defined as no evidence of both primary tumor regrowth and death from any cause, were 91% (95% CI, 81–100%) and 80% (95% CI, 66–95%), respectively (Fig. 1). The corresponding disease progression-free survival rates were 73% (95% CI, 58–87%) and 58% (95% CI, 42–75%), respectively (Fig. 1). The overall survival rate at 2 years was 84% (95% CI, 71–97%) (Fig. 2).

Acute and late toxicities in all patients are shown in Table 2. Acute Grade 1 esophagitis was observed in 1 patient with T2 tumor (Stage IB) near the aortic arch who received a total dose of 88 Gy_E. Acute Grade 1 fever was observed in 1 patient with Stage IB disease who received a total dose of 80 Gy_E. No Grade 2 or greater acute toxicity was observed.

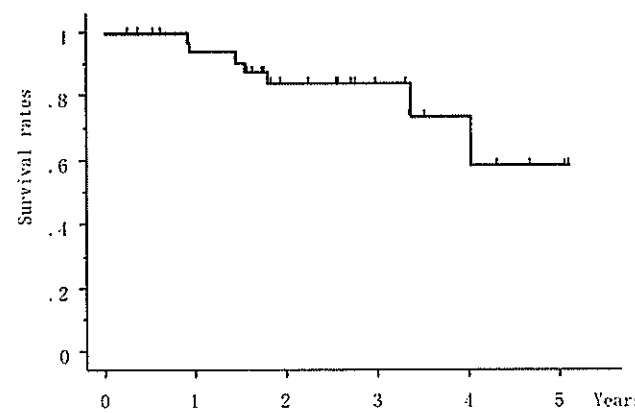

Fig. 2. Overall survival in all patients

Table 2. Acute and late toxicities

Toxicity	Grade	No. of patients
Acute		
Dermatitis	1	29
Esophagitis	1	1
Fever	1	1
Late		
Chest pain	1	4
Pulmonary*	1	25
	2	3
	3	3

* Including radiation pneumonitis and pleural effusion.

Late Grade 1 chest pain, consistent with the proton therapy field, was observed in 4 patients who received 80 or 88 Gy_E. Grade 2 and Grade 3 late pulmonary toxicities were observed in 3 patients each. They received 88 Gy_E of PBT, except for 1 patient who received 94 Gy_E. All Grade 2 pulmonary toxicities were radiation pneumonitis, which occurred from 4.5 to 8 months after the treatment. Two of the late Grade 3 pulmonary toxicities were pleural effusion requiring repeated drainage. One was observed at 9 months and the other at 23 months after treatment, with no evidence of disease progression. The other late Grade 3 pulmonary toxicity was radiation pneumonitis, treated by steroid pulse therapy and oxygen inhalation. It occurred 2.5 months after the beginning of PBT.

Late toxicities by clinical substage are shown in Table 3. Of 6 patients who suffered Grade 2 or greater late pulmonary toxicity, 5 had Stage IB disease.

The patterns of failure by clinical substage are shown in Table 4. Two local tumor regrowths were observed in Stage IB disease. Of the 5 patients who experienced pulmonary hilar or mediastinal lymph node recurrence without primary tumor regrowth, 4 had Stage IB disease. Distant relapse alone occurred equally in Stage IA and Stage IB. The locoregional relapse-free and overall survival curves in Stage IA and Stage IB are shown in Figs. 3 and 4. The 2-year locoregional relapse-free survival rates were 94% (95% CI, 58–100%) in Stage IA and 62% (95% CI, 38–81%) in Stage IB, and the 2-year overall survival rates were 83% (95% CI, 62–100%) in Stage IA and 82% (95% CI, 64–100%) in Stage IB.

Table 3. Late toxicities by clinical stage

Toxicity	All (n = 37)	Stage IA (n = 17)	Stage IB (n = 20)
Chest pain			
Grade 1	4	2	2
Pulmonary			
Grade 1	25	14	11
Grade 2	3	1	2
Grade 3	3	0	3

Table 4. Patterns of failure by clinical stage

Site	All (n = 37)	Stage IA (n = 17)	Stage IB (n = 20)
Local only	1	0	1
Locoregional	1	0	1
Regional only	5	1	4
Regional and distant	1	0	1
Distant only	6	3	3

DISCUSSION

Our results show that PBT is a promising treatment modality for Stage I NSCLC. Although the number of patients was small and the duration of follow-up was short, the 2-year local progression-free and overall survival rates were 80% (95% CI, 66–95%) and 82% (95% CI, 68–97%), respectively. Loma Linda University and Tsukuba University also reported similarly good results of PBT for Stage I NSCLC (11–13). At Loma Linda University, 68 patients were treated by a total dose of 51 Gy_E or 60 Gy_E in 10 fractions, and the 3-year disease-specific survival rate was 72% (12). At Tsukuba University, in 28 Stage I patients (Stage IA/IB, 9/19), the 2-year and 5-year cause-specific survival rates were 66% and 40%, respectively (13).

These results of PBT series are superior to those of conventional radiotherapy, for which 5-year overall survival rates range from only 5% to 30% (3–6). Stereotactic radiotherapy with photon beams, however, has been used to treat Stage I NSCLC in many institutions and produces better outcomes than conventional radiotherapy (14–17). Onishi *et al.* retrospectively reported the results of a Japanese multi-institutional study. The 3- and 5-year cause-specific survival rates were both 78% (17).

Stratifying the results of PBT series by clinical substage, the Loma Linda study showed increased tumor relapse rates in Stage IB patients compared with Stage IA patients (51% vs. 13% at 3 years), and overall survival in Stage IA patients was better than that in Stage IB patients (median survival, 39 months vs. 19 months) (12). Tsukuba University also

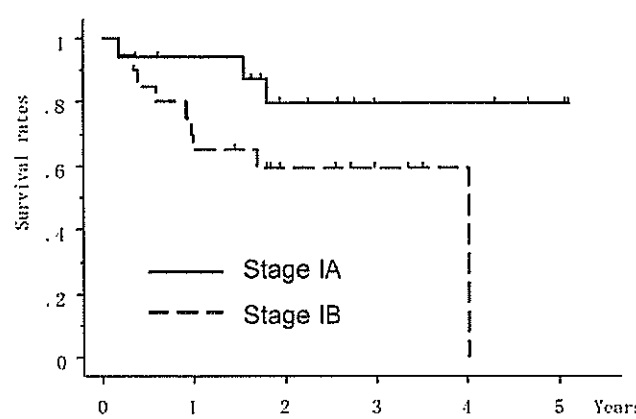

Fig. 3. Locoregional relapse-free survival rates in Stage IA and Stage IB disease.

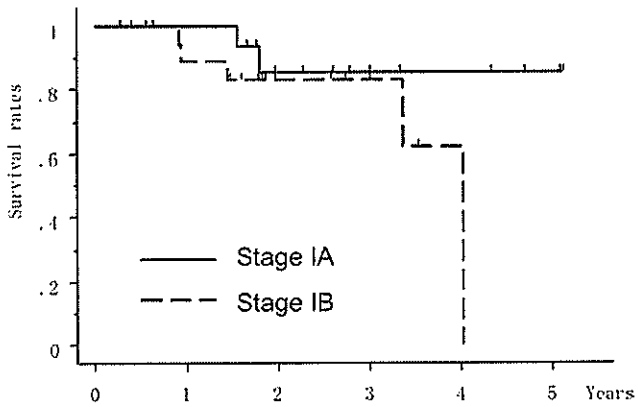

Fig. 4. Overall survival rates in Stage IA and Stage IB disease.

reported that Stage IA patients fared significantly better than did Stage IB patients both in 5-year cause-specific (88% vs. 23%) and disease-free survival rates (89% vs. 17%) (13). Similarly, in the present study, a poorer outcome was observed in Stage IB patients compared with Stage IA patients. Two patients who experienced local tumor regrowth both had Stage IB disease, and locoregional recurrences were observed more frequently in Stage IB disease (30% [95% CI, 12–54%]) than in Stage IA disease (6% [95% CI, 0–28%]) (Table 4, Fig. 3).

Thus, in Stage IA disease, the results of high-dose PBT alone might be comparable to those of surgical series. In Stage IB disease, however, the outcome remains poor. As discussed in the Tsukuba study (13), these results of PBT series in Stage IB patients suggest that clinical Stage IB patients might have had pathologically more advanced disease. The addition of elective nodal irradiation or systemic treatment could eradicate the microscopic nodal or distant diseases. Some randomized trials have recently suggested the significant benefit of adjuvant systemic therapy after surgical resection over surgery alone, even for pathologically proven Stage IB disease (18–20).

Another hypothesis explaining the poor outcomes in Stage IB disease was that the total doses used by the PBT series might be insufficient to control primary tumors. Larger tumors contain more malignant cells and more hypoxic areas, thus requiring higher radiation doses to be controlled. If the malignant disease is confined to the primary site, higher doses focusing on the primary tumor might prevent the malignant cells from metastasizing, thereby improving the outcomes in Stage IB diseases.

The acute toxicities of PBT were acceptable in the current study, as other institutions reported. As for late toxicities, the Loma Linda study reported no radiation pneumonitis requiring steroids or anti-inflammatory therapy (12). At Tsukuba University, among 51 patients with more advanced diseases, there were three Grade 2 and one Grade 3 lung toxicities approximately 3 months or longer after radiotherapy completion (13). In contrast, we experienced substantial late pulmonary toxicities. Six patients, corresponding to 16% (95% CI, 6–32%), suffered Grade 2 or greater late pulmonary toxicities.

One possible reason for the late pulmonary toxicities observed in the present study was that the total doses used in our institution were biologically higher than those used in other institutions. According to the linear–quadratic model, the biologic equivalent dose (BED) is defined as $D(1 + d/\alpha/\beta)$, in which D is the total dose, d is the daily dose, and α/β is assumed to be 10 for tumors. The BEDs for 70/80/88/94 Gy_E used in the current study were 95/112/127/138 Gy_{10}, whereas the BED used in the Loma Linda study was 96 Gy_{10} and those in the Tsukuba study were 90 Gy_{10} for Stage IA and 105 Gy_{10} for Stage IB. Six patients who experienced Grade 2 or greater late pulmonary toxicities in the present study received 88 Gy_E (127 Gy_{10}) or 94 Gy_E (138 Gy_{10}).

Independent of total dose, there are some considerations to explain pulmonary toxicities after PBT. The proton beam should stop at the distal margin of the target volume, but because aerated lung tissue is less dense than other soft tissues of the body, the proton beam might pass through beyond the target volume, and an unexpected high dose area might be generated in the surrounding normal lung. From a biologic viewpoint, because it is suggested that the relative biologic effectiveness of proton beams becomes larger at the distal end of their track, higher biologic lung dose behind the target volume potentially might be associated with the late pulmonary toxicities.

Another consideration is the tumor shrinkage during the treatment period. If overall treatment time is long enough for the tumor to respond to PBT and start shrinking, an aerated space appears where the tumor existed, and the proton beam will deliver excessive doses to the normal lung tissue both around and behind the reduced tumor in the target volume. A hypofractionation approach with a shorter treatment period can avoid this phenomenon. Proton beam therapy in the hypofractionation schedule can be finished before the tumor begins to shrink, and the planned dose should be completely delivered to the target volume. A hypofractionation strategy might be potentially more effective for the tumor and less toxic for the surrounding normal lung. Our PBT schedule required 4 to 5 weeks to complete the treatment, but a shorter overall treatment time with hypofractionation can be considered as a future strategy. Loma Linda University has been using a 2-week/10-fraction schedule, and some Japanese stereotactic radiotherapy institutions have already experienced shorter treatment schedules, within 1 week (12, 14, 15).

Another concern with late pulmonary toxicities is the target volume. Of 6 patients who developed Grade 2 or greater pulmonary toxicities, 5 had Stage IB disease. As the target volume increases, naturally the volume of the irradiated normal lung becomes larger, and the risk of pulmonary toxicities gets higher.

From these findings and discussions, the PBT schedule for Stage IB patients should be reconsidered. As discussed above, if the malignant cells are confined to the primary tumor, higher doses to the primary tumor can lead to better

local tumor control and reduce both locoregional and distant relapse in Stage IB diseases; but in contrast, it also includes more risk of generating pulmonary toxicities. Therefore, although there might be an opportunity for further dose escalation for Stage IB disease, it should be cautiously examined only on a prospective clinical study basis.

In Stage IA patients, the results of high-dose PBT alone might be comparable to those of surgical series. To further enhance its efficacy and reduce its toxicity, a hypofractionation schedule is considered to be a promising future strategy. More data from prospective clinical trials will be needed to confirm the benefit of PBT in the future.

REFERENCES

1. Ginsgerg RJ, Rubinstein LV. Randomized trial of lobectomy versus limited resection for T1 N0 non-small cell lung cancer. Lung Cancer Study Group. *Ann Thorac Surg* 1995;60:615–622.
2. Adebonojo SA, Bowser AN, Moritz DM, *et al.* Impact of revised stage classification of lung cancer on survival: a military experience. *Chest* 1999;115:1507–1513.
3. Harpole DH Jr., Herndon JE Jr., Young WG, *et al.* Stage I nonsmall cell lung carcinoma. A multivariate analysis of treatment methods and patterns of recurrence. *Cancer* 1995;76: 787–796.
4. Martini N, Bains MS, Burt ME, *et al.* Incidence of local recurrence and second primary tumors in resected stage I lung cancer. *J Thorac Cardiovasc Surg* 1995;109:120–129.
5. Graham PH, Gebski VJ, Langlands AO. Radical radiotherapy for early non–small-cell lung cancer. *Int J Radiat Oncol Biol Phys* 1995;31:261–266.
6. Mehta M, Scrimger R, Mackie R, *et al.* A new approach to dose escalation in non–small-cell lung cancer. *Int J Radiat Oncol Biol Phys* 2001;49:23–33.
7. Zimmermann FB, Bamberg M, Molls M, *et al.* Radiation therapy alone in early stage non-small cell lung cancer. *Semin Surg Oncol* 2003;21:91–97.
8. Ogino T, Murayama S, Itou Y, *et al.* Three-dimensional positioning verification by image subtraction method using real-time digital radiography [Abstract]. *Int J Radiat Oncol Biol Phys* 2000;48(Suppl. 1):195.
9. Ando K, Furusawa Y, Suzuki M, *et al.* Relative biological effectiveness of the 235 MeV proton beams at the National Cancer Center Hospital East. *J Radiat Res* 2001;42:79–89.
10. Therasse P, Arbuck SG, Eisenhauer EA, *et al.* New guidelines to evaluate the response to treatment in solid tumors. *J Natl Cancer Inst* 2000;92:205–216.
11. Bush DA, Slater JD, Bonnet R, *et al.* Proton-beam radiotherapy for early-stage lung cancer. *Chest* 1999;116:1313–1319.
12. Bush DA, Slater JD, Shin BB, *et al.* Hypofractionated proton beam radiotherapy for stage I lung cancer. *Chest* 2004;126: 1198–1203.
13. Shioyama Y, Tokuuye K, Okumura T, *et al.* Clinical evaluation of proton radiotherapy for non–small-cell lung cancer. *Int J Radiat Oncol Biol Phys* 2003;56:7–13.
14. Uematsu M, Shioda A, Suda A, *et al.* Computed tomography-guided frameless stereotactic radiotherapy for Stage I non–small-cell lung cancer: A 5-year experience. *Int J Radiat Oncol Biol Phys* 2001;51:666–670.
15. Nagata Y, Negoro Y, Aoki T, *et al.* Clinical outcomes of 3D conformal hypofractionated single high-dose radiotherapy for one or two lung tumors using a stereotactic body frame. *Int J Radiat Oncol Biol Phys* 2002;52:1041–1046.
16. Timmerman R, Papiez L, McGarry R, *et al.* Extracranial stereotactic radioablation. Results of a phase I study in medically inoperable stage I non-small cell lung cancer. *Chest* 2003;124:1946–1955.
17. Onishi H, Araki T, Shirato H, *et al.* Stereotactic hypofractionated high-dose irradiation for stage I nonsmall cell lung carcinoma. Clinical outcomes in 245 subjects in a Japanese mutiinstitutional study. *Cancer* 2004;101:1623–1631.
18. Winton TL, Livingston R, Johnson D, *et al.* National Cancer Institute of Canada Clinical Trials Group. National Cancer Institute of the United States Intergroup JBR. 10 Trial Investigators. Vinorelbine plus cisplatin vs. observation in resected non-small cell lung cancer. *N Engl J Med* 2005;352:2589–2597.
19. Strauss GM, Herndon J, Maddaus MA, *et al.* Randomized clinical trial of adjuvant chemotherapy with paclitaxel and carboplatin following resection in stage IB non-small cell lung cancer (NSCLC): Report of Cancer and Leukemia Group B (CALGB) Protocol 9633 [Abstract]. *Proc Am Soc Clin Oncol* 2004;7019.
20. Kato H, Ichinose Y, Ohta M, *et al.* A randomized trial of adjuvant chemotherapy with uracil-tegafur for adenocarcinoma of the lung. *N Eng J Med* 2004;350:1713–1721.

INSTITUTE OF PHYSICS PUBLISHING PHYSICS IN MEDICINE AND BIOLOGY

Phys. Med. Biol. 51 (2006) 1249–1260 doi:10.1088/0031-9155/51/5/014

Development of a simple control system for uniform proton dose distribution in a dual-ring double scattering method

Teiji Nishio[1], Shouji Kataoka[2], Masanori Tachibana[2], Kazutomo Matsumura[3], Naoya Uzawa[3], Hideki Saito[3], Toshinobu Sasano[4], Michiharu Yamaguchi[4] and Takashi Ogino[1]

[1] Particle Therapy Division, Research Center for Innovative Oncology, National Cancer Center, Kashiwa, Japan
[2] Sumitomo Heavy Industries Ltd, Japan
[3] SHI Accelerator Service Ltd, Japan
[4] Accelerate Engineering Company, Japan

Received 21 October 2005, in final form 26 December 2005
Published 15 February 2006
Online at stacks.iop.org/PMB/51/1249

Abstract

In proton radiotherapy with high focusing of irradiation on the tumour, it is important to obtain treatment beams with a highly uniform dose distribution. Uniform dose distribution in the clinical irradiation field can be obtained by the dual-ring double scattering method. This method is superior to the wobbler method, which uses electromagnetic deflection of the proton beams, because of the absence of the temporal structure of irradiation distribution. However, in the dual-ring double scattering method the condition of incident proton beams entering the scatter, especially the accuracy of the position of the incident proton beams with respect to the scatter, markedly affects the uniformity of the beam distribution in the irradiation field. In this study, to ensure the uniformity of dose distribution during treatment, we developed a control system equipped with an automatic fine adjustment of the beam axis and a mechanism for moving the second dual-ring scatter of the double scatters to the optimal position. Using this system, we achieved uniform dose distribution in the irradiation field during proton radiotherapy, with symmetry within ±1% and flatness within 2%.

(Some figures in this article are in colour only in the electronic version)

1. Introduction

Recently, radiotherapy using heavy-charged particle beams, such as proton beams and carbon beams, has been spreading throughout Japan and the world (PTCOG Newsletter 2004). Since heavy-charged particles have a charge, the beams are deflected in electromagnetic fields, and

0031-9155/06/051249+12$30.00

multiple scattering and energy loss due to the Coulomb force occur when passing through substances. These properties are utilized for the formation of the irradiation field used for radiotherapy. In an irradiation field, uniformity of depth–dose distribution is formed by the bar-ridge filter or range modulator using energy loss resulting from the passing of particles through substances. The dual-ring double scattering method or wobbler method is used for a uniformly lateral dose distribution (Chu *et al* 1993, Graffman *et al* 1973, Koehler *et al* 1977).

In the proton radiotherapy facility of the National Cancer Center, Kashiwa, there are small-size normal conduction AVF cyclotron (C235) for medical purposes, two rotating gantry ports and one horizontal fixed port (Nishio 1999, Tachikawa *et al* 1999). To obtain laterally uniform irradiation fields, the dual-ring double scattering method is used in one rotating gantry port and the horizontal fixed port, and the wobbler method is used in the other rotating port.

To achieve uniform dose distribution in the irradiation field, the dual-ring double-scattering method requires much stricter initial conditions of incident beams entering the irradiation apparatus than the wobbler method (Takada 1994, 2002). If a rotating gantry is equipped, vertical sag due to the weight of the gantry affects the accuracy of the positions of each device. To achieve uniform dose distribution in the irradiation field and high reproducibility of the initial condition of beams, we developed a control system equipped with a mechanism for automatic fine adjustment of the beam incidence position and movement of the second dual-ring scatter to the optimal position.

2. Material and method

2.1. Apparatus for the formation of the irradiation field

The dual-ring double-scattering method consists of a profile monitor, a dual-ring double-scattering system, ring collimator (RC), ridge filter (RF), fine degrader (FD), dose monitor, flatness monitor, block collimator (BC), patient bolus (PB) and patient collimator (PC) (figure 1). Spread-out Bragg peak (SOBP) for the uniform dose distribution in the depth direction, which is produced by the aluminium wedge-shaped RF, can be selected from 8 grades between 30 mm and 100 mm in 10 mm steps for treatment. The FD is for the fine adjustment of the range to the target in the patient's body, the dose monitor is for the determination of the irradiation absolute dose, the flatness monitor is for the confirmation of the dose uniformity during irradiation of treatment beams, and the patient bolus and collimator are used for the shaping of beams based on the tumour size and form in each patient. Parameters for the formation of the individual irradiation field, SOBP, FD thickness, dose monitor value and patient bolus/collimator are determined for each patient and irradiation field.

The dual-ring double-scattering system of our centre is equipped with a uniform scatter made of Pb (first scatter) with variable thickness on the beam upstream side and another scatter with a dual-ring structure, the inner ring of which is made of Pb, and the outer one of Al (second scatter) on the beam downstream side. The thickness of the first scatter and the shape of the second scatter are determined by the energy of the proton beams. The second scatter can be moved three-dimensionally from 0 mm to 10 mm on the X- and Y-axis with the standard position, X, $Y = 5$ mm, and -100 mm to $+100$ mm on the Z-axis by remote control (see the dashed frame of figure 1). The maximum size of the irradiation field provided by the dual-ring double-scattering systems in the rotating gantry port is 200 mm ϕ.

The profile monitor consists of 8 air ionization dosimeters in the shape of a fan with 1/8 circle and is used for the observation of incidence proton beam axis and shape. The flatness

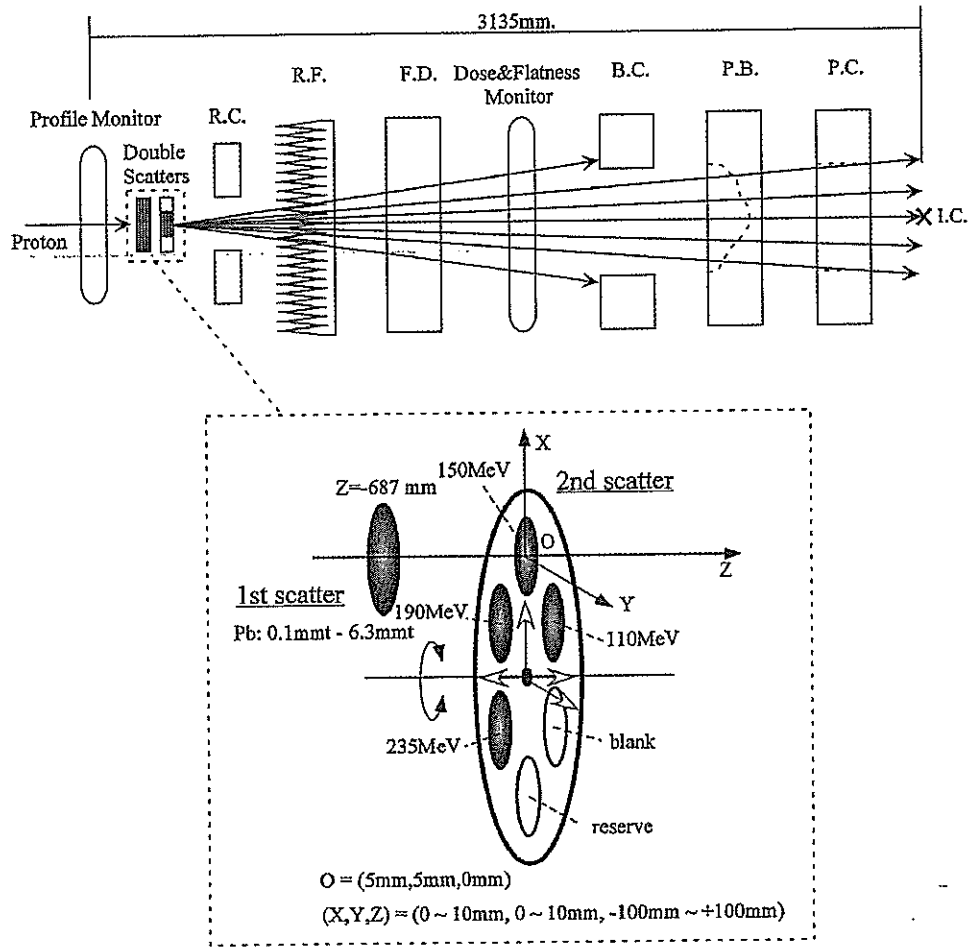

Figure 1. Arrangement of apparatus parts for the dual-ring double-scattering method.

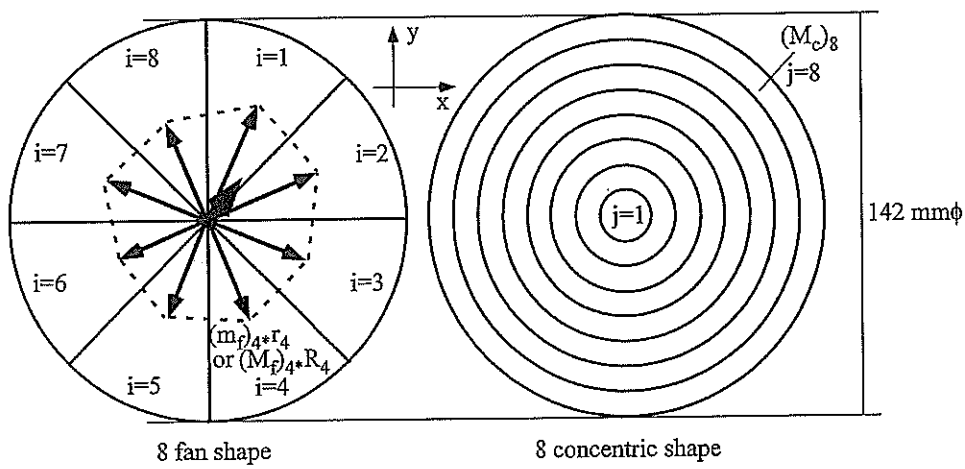

Figure 2. Illustration of the profile and flatness monitors.

monitor for the observation of uniformity of lateral dose distribution has a two-layer structure, with one layer consisting of 8 fan-shaped air ionization dosimeters (same shape as the profile monitor) and the other being 8 concentric air ionization dosimeters. The detailed shapes of the profile and flatness monitors are illustrated in figure 2. Profile monitor indication (PMI)

and flatness monitor indication (FMI) are defined as

$$\overrightarrow{\mathrm{PMI}}(I_f : x, y) = \sum_{i=1}^{8} (m_f)_i \cdot \vec{r}_i(x_i, y_i) = \begin{cases} \sum_{i=1}^{8} (m_f)_i \cdot x_i \\ \sum_{i=1}^{8} (m_f)_i \cdot y_i \end{cases}$$
$$= \begin{cases} \mathrm{PMI}(I_f : x) \\ \mathrm{PMI}(I_f : y) \end{cases}, \quad |\vec{r}_i| = 1 \text{ (8 fan shape)}, \tag{1}$$

$$\begin{cases} \overrightarrow{\mathrm{FMI}}(I_f : x, y) = \sum_{j=1}^{8} (M_f)_j \cdot \vec{R}_j(x_j, y_j) = \begin{cases} \sum_{j=1}^{8} (M_f)_j \cdot x_j \\ \sum_{j=1}^{8} (M_f)_j \cdot y_j \end{cases} \\ \qquad = \begin{cases} \mathrm{FMI}(I_f : x) \\ \mathrm{FMI}(I_f : y) \end{cases}, \qquad |\vec{R}_j| = 1 \text{ (8 fan shape)}, \\ \mathrm{FMI}(I_c) = \sum_{k=1}^{8} \left| \dfrac{(M_c)_k}{(M_c)_1 \cdot (2 \cdot k - 1)} - 1 \right| \qquad \text{(8 concentric shape)}. \end{cases} \tag{2}$$

Here, i, j and k denote identification of 8 fan and concentric separated areas, respectively. m_f, M_f and M_c are output signals from each separated area. In the profile monitor, the centre and symmetry are indicated by the length of the thick vector, $\mathrm{PMI}(I_f : x, y)$ and the shape formed with 8 thin vectors, $(m_f)_j \cdot r_j$, shown in figure 2. The beam approaches a centre position of the profile monitor as the length of the thick vector shortens. Similarly, in the flatness monitor, the symmetry and flatness of the dose profile are indicated by the length of the thick vector, $\mathrm{FMI}(I_f : x, y)$, and the value of $\mathrm{FMI}(I_c)$.

2.2. Measurement of relationship between the incident beam conditions and uniformity of the dose distribution

The dose distribution optimized in an irradiation field of 200 mm ϕ by the dual-ring double-scattering method is formed by the following equations (Takada 2002):

$$F(r) = f_{\mathrm{inner}}(r) + f_{\mathrm{outer}}(r),$$
$$f_{\mathrm{inner}}(r) = 1.80 \times 10^{-9} \cdot \exp(-8.90 \times 10^{-5} \cdot r^2) \int_0^{90} k \cdot \exp(-1.89 \times 10^{-4} \cdot k^2) \times \left[\int_0^{\pi} \exp(1.78 \times 10^{-4} \cdot r \cdot k \cdot \cos\theta)\, \mathrm{d}\theta \right] \mathrm{d}k,$$
$$f_{\mathrm{outer}}(r) = 1.06 \times 10^{-8} \cdot \exp(-5.22 \times 10^{-4} \cdot r^2) \int_{90}^{\infty} k \cdot \exp(-6.22 \times 10^{-4} \cdot k^2) \times \left[\int_0^{\pi} \exp(1.04 \times 10^{-3} \cdot r \cdot k \cdot \cos\theta)\, \mathrm{d}\theta \right] \mathrm{d}k. \tag{3}$$

Here, $f_{\mathrm{inner}}(r)$ and $f_{\mathrm{outer}}(r)$ denote the dose distribution components by the inner and outer rings of the second scatter, respectively, and r denotes the distance from the centre of the beam axis. Table 1 shows the conditions of the first and second scatters at each beam energy of 150 MeV, 190 MeV and 235 MeV. To obtain a dose distribution with a high degree of uniformity in the irradiation field, stability of the beam incidence position at the dual-ring scatter is very important.

The depth and lateral dose distribution for beam energies of 150, 190, 235 MeV, each SOBP, and FD in the field size of 200 mm are measured by changing the incident beam condition in the irradiation equipment. The measurement of the dose distribution is performed using a three-dimensional (3D) water phantom and an ionization chamber with a sensitive

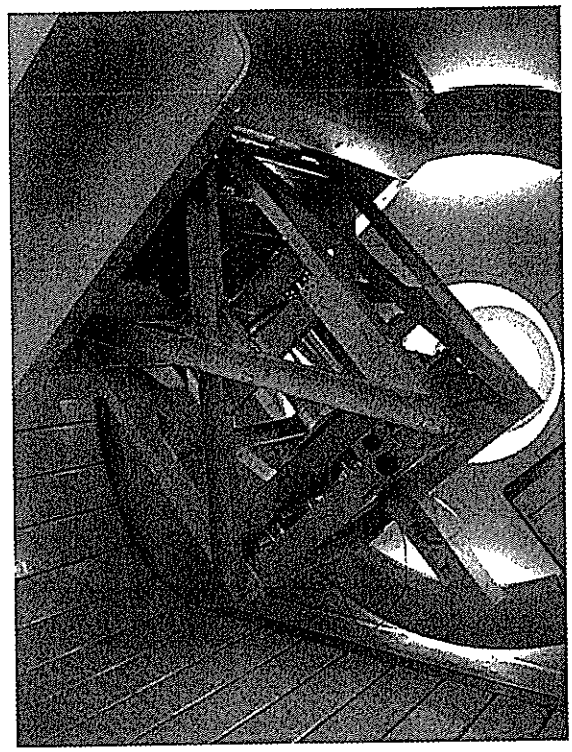

Figure 3. Picture of 3D water phantom.

Table 1. Thickness and characteristics of the first and second scatters.

Energy (MeV)	First scatter (Pb) thickness (mm)	Inside second scatter (Pb) thickness (mm)	Inside second scatter (Pb) diameter (mm)	Outside second scatter (Al) thickness (mm)
150	1.5	2.952	27.48	7.997
190	2.3	4.038	25.58	11.087
235	3.5	5.314	24.00	14.760

volume of 75 μl (figure 3). The 3D water phantom can rotate together with a nozzle of the rotating gantry. The depth and lateral dose distribution are measured by 1 mm and 2 mm step s^{-1}, respectively.

The uniformity of the measured lateral dose distribution was evaluated using parameters defined by the following symmetry and flatness (IEC 1989):

$$\text{Uniformity} = \begin{cases} \text{Symmetry} : S_{\text{FWHM}}\,[\%] = \dfrac{A_+ - A_-}{A_+ + A_-} \times 100, \\ \text{Flatness} : F_{0.8\times\text{FWHM}}\,[\%] = \dfrac{D_{\max} - D_{\min}}{D_{\max} + D_{\min}} \times 100. \end{cases} \tag{4}$$

The symmetry is expressed as the difference between the area on the '+' side of the lateral position (A_+) and the area on the '$-$' side of the lateral position (A_-) within an area of full-width at half-maximum (FWHM). The flatness is expressed as the difference between the maximal radiation dose ($D_{\max}$) and the minimal radiation dose ($D_{\min}$) within an area of 80% FWHM. The IEC (1989) report recommends symmetry of less than $\pm 2\%$ and flatness of less than 5%. However, the symmetry and flatness for proton radiotherapy are not regulated. In this study,

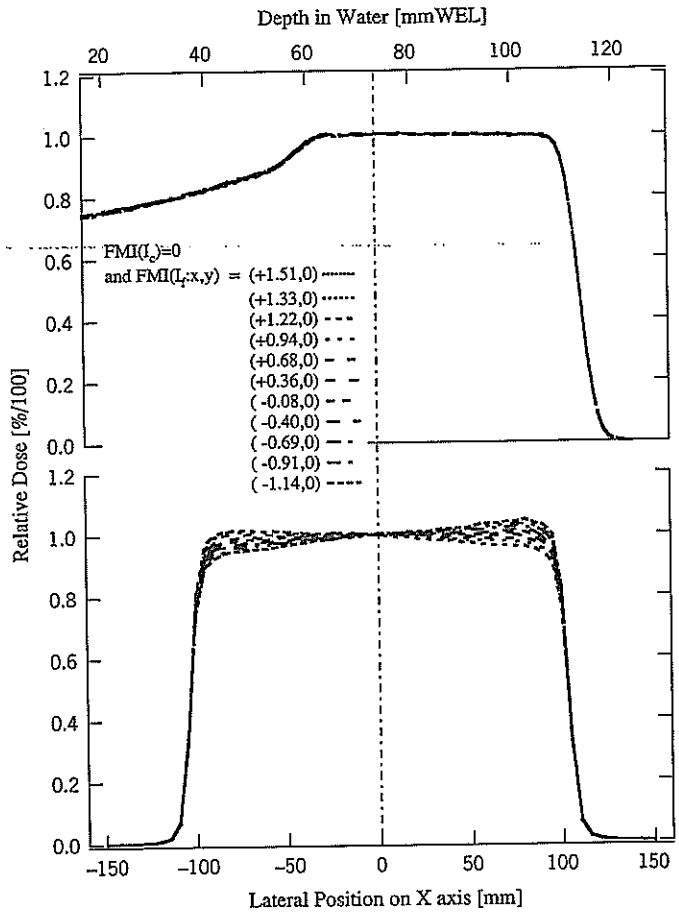

Figure 4. Depth and X-axis lateral dose distributions measured at $\overrightarrow{\mathrm{FMI}}(I_f : x, y) = (\mathrm{FMI}(I_f : x), 0)$ with $\mathrm{FMI}(I_c) \approx 0$ under the conditions of 150 MeV/SOBP 50 mm/Gantry = 0°.

we used symmetry of less than ±1% and flatness of less than 2.5% for the evaluation of proton radiotherapy.

3. Results and discussions

3.1. Correlation between the flatness monitor indication and uniformity of the dose distribution

The uniformity of the dose distribution in proton radiotherapy is observed using a flatness monitor. Figure 4 shows the depth and lateral dose distribution on the central axis of an SOBP measured at $\overrightarrow{\mathrm{FMI}}(I_f : x, y) = (-1.14, 0) \leftrightarrow (+1.51, 0)$ and $\mathrm{FMI}(I_c) \approx 0$ under the conditions of 150 MeV/SOBP 50 mm/Gantry = 0°. Figure 5 shows the symmetry and flatness of the lateral dose distribution measured at the flatness monitor indications under the conditions of 150 MeV/SOBP 50 mm/Gantry = 0°, 190 MeV/SOBP 80 mm/Gantry = 0° and 235 MeV/SOBP 80 mm/Gantry = 0°. These findings indicated that the uniformity of the dose distribution decreased by changing the $\overrightarrow{\mathrm{FMI}}(I_f : x, y)$ from the standard: $\overrightarrow{\mathrm{FMI}}(I_f : x, y) \approx (0, 0)$ and $\mathrm{FMI}(I_c) \approx 0$.

To satisfy a symmetry of less than ±1% and flatness of less than 2.5% in the dose distribution for proton radiotherapy, the $\mathrm{FMI}(I_f : x)$ and $\mathrm{FMI}(I_f : y)$ must be within ±0.03, respectively. Since no differences in the shape of the depth–dose distribution under different beam conditions were observed, it was not discussed in this study.

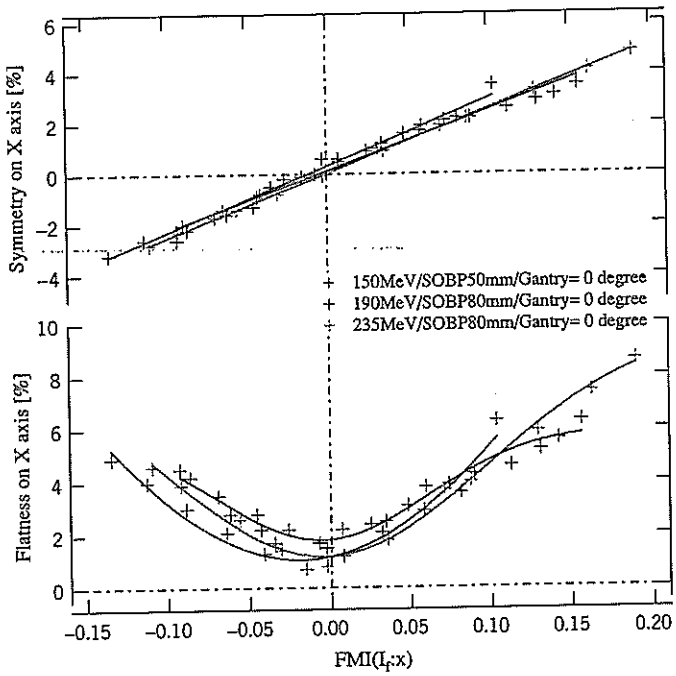

Figure 5. Symmetry and flatness of the X-axis lateral dose distribution measured at $\overrightarrow{\mathrm{FMI}}(I_f : x, y) = (\mathrm{FMI}(I_f : x), 0)$ with $\mathrm{FMI}(I_c) \approx 0$ under the conditions of 150 MeV/SOBP 50 mm/Gantry = 0°, 190 MeV/SOBP 80 mm/Gantry = 0°, and 235 MeV/SOBP 80 mm/Gantry = 0°.

3.2. Correlation between the profile monitor indication and the uniformity of the dose distribution with changes in the second scatter position

Figure 6 shows the uniformity of the dose distribution by mechanically moving the second scatter in 0.4 mm steps from the scatter position (−6 mm) with the initial beam condition for the uniform dose profile: $\overrightarrow{\mathrm{FMI}}(I_f : x, y) = (0, 0)$ and $\mathrm{FMI}(I_c) \approx 0$. Only the second scatter was moved in the constant beam condition ($\overrightarrow{\mathrm{FMI}}(I_f : x, y) \neq (0, 0)$). The movement value of the second scatter corresponded to the difference between the positions of the second scatter centre and the large Gaussian beam centre passing through the first scatter by the principle of the dual-ring double-scattering method. The uniformity of the dose distribution for proton radiotherapy is satisfied when the difference is less than 1 mm between the positions of the second scatter centre and the beam centre axis.

3.3. Correlation between the second scatter position and the profile monitor indication

The top graph of figure 7 shows the correlation between the incidence position of the beam observed by the profile monitor and the second scatter position. The second scatter was moved in a plane perpendicular to the beam axis so that the $\overrightarrow{\mathrm{FMI}}(I_f : x, y) = (0, 0)$ to the incidence beams. In the range of $|\overrightarrow{\mathrm{PMI}}(I_f : x, y)| \leqslant (1.0, 1.0)$, there was a linear correlation between the positions of the second scatter and incidence beams.

The middle and bottom graphs show the symmetry and flatness of the dose distribution with the second scatter position evaluated using equation (3). The results shown in figure 7 indicated that the flatness of the dose distribution required the $|\overrightarrow{\mathrm{PMI}}(I_f : x, y)| < (0.5, 0.5)$ and the second scatter position of 3–7 mm. The changes in the symmetry and flatness of the dose distribution caused by moving the second scatter were slower than those shown in figure 6. The beam centre always matches with the second scatter centre by movement